

# Outer-Loop Control Law Design with Control Allocation for a Multibody Aircraft

Alexander Köthe, Robert Luckner

**Abstract** In recent years, unmanned aircraft used as High-Altitude Platform Systems have been studied in research and industry as alternative technologies to satellites. Regarding actual operation and flight performance of such systems, a linked formation of multiple aircraft, so called multibody aircraft, seem to be a promising aircraft configuration. In terms of flight dynamics, those aircraft strongly differ from classical rigid-body and flexible aircraft, because a strong interference between flight mechanic and formation modes occurs. An inner-loop flight control law provides a frequency separation of both mode groups. The inner loop holds the shape of the formation and transforms the multibody aircraft to a conventional aircraft in terms of flight dynamics, however, particular characteristics exist, like flying with airspeed close to stall and the extremely large wingspan, which have to be considered for manoeuvring and in the outer-loop flight control law design. In addition, the multibody aircraft is an over-actuated system. This paper describes the outer loop flight control law design for flight path tracking of a multibody aircraft with control allocation. The presented method can be adopted to any other high-aspect ratio aircraft with similar dynamics.

## 1 Introduction

Aircraft operating as so-called High-Altitude Platform Systems (HAPS) have been considered as a complementary technology to satellites since several years. A suitable HAPS aircraft configuration is the so-called *multibody aircraft*. The concept assumes multiple aircraft connected to each other at their wingtips. The idea dates back to the German engineer Dr. Vogt [10]. In the United States, shortly after the

---

Alexander Köthe · Robert Luckner  
Technische Universität Berlin, Marchstraße 12, 10587 Berlin, Germany  
alexander.koethe@ilr.tu-berlin.de,  
robert.luckner@tu-berlin.de

end of World War II, Vogt experimented with the coupling of manned aircraft. This resulted in a high-aspect-ratio wing for the overall aircraft formation. The range of the formation could be increased correspondingly. The engineer Geoffrey S. Sommer took up Vogt's idea and patented an aircraft configuration consisting of several unmanned aerial vehicles coupled at their wingtips [13]. A flight mechanical analysis (static and dynamic) and the design of flight control laws is missing in Sommer's patent.

In the internal TU Berlin project *AlphaLink*, the flight mechanic design, the flight dynamic modelling and the flight control laws for a multibody aircraft configuration were established. From a flight control point of view, the designed multibody aircraft has some special characteristics:

1. The *formation modes* that occur due to the mechanical wing tip connection do not have any mechanical stiffness or damping and, hence, their eigenvalue and eigenvector characteristics only depend on the aerodynamics. This leads to low eigenfrequencies and a strong coupling between rigid-body modes and formation modes.
2. The designed aircraft is a formation of 10 single aircraft. The equations of motion have 50 inputs, but only 24 degrees of freedom. Hence, a suitable control allocation is required.
3. The multibody aircraft operates close to stall speed to reduce the required power, which is necessary to fulfill the energy balance between available sun energy and required propulsion energy.
4. The wingspan of the aircraft is very high. Non-uniformly distributed gust can occur and, in combination with the operational airspeed, the bank angle and the yaw rate in turns are limited.

The first and second issues mentioned above are already solved [8].<sup>1</sup> This paper presents the design of the outer loops for flight path control taking the low airspeed and large wingspan into account. A control allocation already exists for the inner loop, but a new solution of the control allocation problem is required while taking the outer-loop flight control laws into account. The presented design method is universally valid for any highly-flexible, high-aspect ratio aircraft configuration.

## 2 Reference Aircraft

This section provides the design parameter of the reference aircraft and describes its flight dynamic characteristics.

---

<sup>1</sup> This paper forms the second part of a set of two papers studying the flight control law design for multibody aircraft. The first paper has also been submitted as contribution to the EuroGNC 2019.

## 2.1 Aircraft Design

The multibody aircraft was designed to achieve the following design requirements, derived in part from the U.S. DARPA<sup>2</sup> *Vulture* program:

- Payload capacity shall be 450 kg and the required payload power is 5 kW.
- The aircraft shall continuously operate for at least one year in the mission altitude of 20,000 m.
- The design operation latitude is specified at 40° N/S.
- The single aircraft shall be able to fly to the mission altitude and to leave the formation in order to return to ground on its own.
- The single aircraft shall be designed as rigid aircraft.

Tab. 1 lists the design properties. Particularly noticeable is the large wing span with 211 m and the low airspeed. The design lift coefficient corresponds to 90 % of the maximum lift coefficient. For the design, a planar wing formation is selected, i.e. a configuration where all individual aircraft have the same bank and pitch angle. Fig. 1 shows the design of such an aircraft configuration. The aircraft are connected by mechanical joints with free motion that allow a pitch and roll motion. Fig. 2 shows the free-body diagram for the selected joint configuration. With this, the formation of ten coupled aircraft consist of

Table 1: Selected parameters for the optimized multibody aircraft with planar wing

Span [m]	210.66				
Aspect ratio [1]	55				
Total mass [kg]	4509				
Total battery mass [kg]	1137				
Altitude [m]	20,000				
Airspeed [m s <sup>-1</sup> ]	33.37				
Horizontal tail area [m <sup>2</sup> ]	6.05				
Vertical tail area [m <sup>2</sup> ]	1.45				
Zero drag coefficient [1]	0.008				
Available sun energy per day [GJ/day]	11.12				
Required sun energy per day [GJ/day]	11.12				
Max. engine power [kW]	11.51				
Long. CG position [m]	-3.74				
Neutral point wing [m]	-3.26				
Distance wing tail [m]	11.49				
Half span per aircraft [m]	10.53				
	AC1	AC2	AC3	AC4	AC5
Angle of attack [1°]	4.8	4.8	4.8	4.8	4.8
Elevator deflection [1°]	-3.58	-6.05	-6.4	-6.51	-6.55
Trim engine power [kW]	5.29	2.04	1.49	1.29	1.22
Lat. CG position [m]	1.69	2.12	1.68	1.05	0.36
Battery shift [m]	6.7	8.39	6.65	4.17	1.42

<sup>2</sup> United States Defense Advanced Research Projects Agency

- **6** rigid-body degrees of freedom and
- **24** degrees of freedom (pitch and roll for every aircraft that is additionally coupled to the reference aircraft) caused by the joint connection.



Fig. 1: Reference aircraft configuration

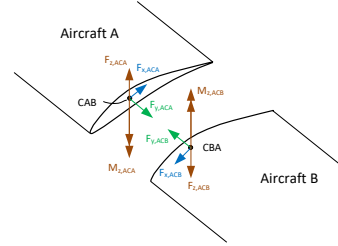


Fig. 2: Reaction forces and moments for a joint with pitch and roll degree of freedom between two aircraft

## 2.2 Flight Dynamics

The equations of motion are derived using Kane's method [5]. Details can be found in Ref. [7]. The fifth aircraft of the formation is selected as reference aircraft. After linearization, the state-space system

$$\begin{aligned}\dot{\mathbf{x}}(t) &= \mathbf{A} \mathbf{x}(t) + \mathbf{B} \mathbf{u}(t) + \mathbf{E} \mathbf{z}(t), \\ \mathbf{y}(t) &= \mathbf{C} \mathbf{x}(t) + \mathbf{D} \mathbf{u}(t) + \mathbf{F} \mathbf{z}(t)\end{aligned}\quad (1)$$

represents a system of linear first-order differential equations with  $\mathbf{A}$  as system matrix,  $\mathbf{B}$  as input matrix,  $\mathbf{E}$  as disturbance matrix,  $\mathbf{C}$  as output matrix,  $\mathbf{D}$  as feedforward matrix and  $\mathbf{F}$  as feedforward disturbance matrix [9]. The state-vector contains

1. Pitch rate  $q$ , angle of attack  $\alpha$ , airspeed  $V_A$ , pitch angle  $\Theta$ , yaw rate  $r$ , sideslip angle  $\beta$ , roll rate  $p$  and bank angle  $\Phi$  for the reference aircraft and
2. Pitch rate  $q_i$ , pitch angle  $\Theta_i$ , roll rate  $p_i$  and bank angle  $\Phi_i$  for all other aircraft  $i$ .

The elevator deflection  $\eta$ , the left  $\xi_{\text{left}}$  and right  $\xi_{\text{right}}$  aileron deflections, the rudder  $\zeta$  and the thrust  $F$  of every aircraft are used as input variables. In summary, 50 input variables are available. The vertical wind is considered as disturbance with a local wind angle of attack  $\alpha_w$ . This leads to 10 disturbance variables. The output variables are equal to the states.

The resulting properties of the eigenvalues ( $\lambda$  as eigenvalue,  $\omega_0$  as undamped eigenfrequency,  $D$  as damping ratio,  $T$  as time constant and  $T_2$  as double time) are listed in Tab. 2. The rigid-body modes are identified with the help of the eigenvectors. The pitch mode, phugoid and spiral eigenvalues can be detected, while an

Table 2: Eigenvalues and corresponding motions for the multibody aircraft. (Kinds of motion: PM - pitch motion, SP - spiral mode, PH - phugoid, AFM – anti-symmetrical formation mode, SFM – symmetrical formation mode)

Mode	Eigenvalue	$\omega_0$ [ $\frac{\text{rad}}{\text{s}}$ ]	$D$ [1]	$T$ [s]	$T_2$ [s]	Motion
1	$\lambda_1 = -1.81$	-	-	0.553	-	AFM
2	$\lambda_2 = -1.74$	-	-	0.575	-	AFM
3	$\lambda_3 = -1.44$	-	-	0.696	-	PM
4	$\lambda_4 = -0.796$	-	-	1.26	-	PM
5	$\lambda_{5,6} = -0.335 \pm j 0.619$	0.703	0.476	-	-	AFM
6	$\lambda_{7,8} = -0.192 \pm j 0.615$	0.645	0.298	-	-	AFM
7	$\lambda_9 = -0.0964$	-	-	10.4	-	SFM
8	$\lambda_{10,11} = -0.205 \pm j 0.59$	0.625	0.328	-	-	AFM
9	$\lambda_{12,13} = -0.601 \pm j 0.579$	0.835	0.72	-	-	AFM
10	$\lambda_{14,15} = -0.604 \pm j 0.537$	0.808	0.747	-	-	AFM
11	$\lambda_{16,17} = -0.178 \pm j 0.424$	0.459	0.387	-	-	AFM
12	$\lambda_{18,19} = 0.284 \pm j 0.408$	0.497	-0.57	-	2.44	AFM
13	$\lambda_{20,21} = -0.262 \pm j 0.394$	0.473	0.553	-	-	AFM
14	$\lambda_{22,23} = -0.738 \pm j 0.357$	0.82	0.9	-	-	AFM
15	$\lambda_{24,25} = -0.541 \pm j 0.278$	0.608	0.889	-	-	SFM
16	$\lambda_{26,27} = 0.188 \pm j 0.26$	0.32	-0.59	-	3.69	SFM
17	$\lambda_{28,29} = 0.172 \pm j 0.224$	0.282	-0.61	-	4.04	AFM
18	$\lambda_{30,31} = 0.0484 \pm j 0.196$	0.201	-0.24	-	14.32	SFM
19	$\lambda_{32,33} = -1.65 \pm j 0.185$	1.66	0.994	-	-	AFM
20	$\lambda_{34,35} = -1.66 \pm j 0.178$	1.67	0.994	-	-	AFM
21	$\lambda_{36,37} = -0.022 \pm j 0.107$	0.109	0.201	-	-	AFM
22	$\lambda_{38,39} = -0.0826 \pm j 0.1$	0.13	0.636	-	-	PH
23	$\lambda_{40,41} = -1.69 \pm j 0.0732$	1.69	0.999	-	-	AFM
24	$\lambda_{42,43} = -1.63 \pm j 0.0562$	1.63	0.999	-	-	AFM
25	$\lambda_{44} = -0.00774$	-	-	129	-	SP

identification of the roll mode and the dutch roll is not unequivocally possible. The remaining modes are stated as formation modes. A clear separation between formation modes and rigid-body modes is not possible. There are six unstable complex conjugate eigenvalues (three modes).

### 3 Flight Control Law Design

The top-level requirements for the flight control laws of the multibody aircraft are i) reaching and holding an altitude, ii) reaching and holding a heading, iii) holding speed to avoid stall and iv) gust rejection. Fig. 3 shows a control law structure that is suitable to achieve those requirements. The detailed design requirements and every component of the flight control law structure is explained next.

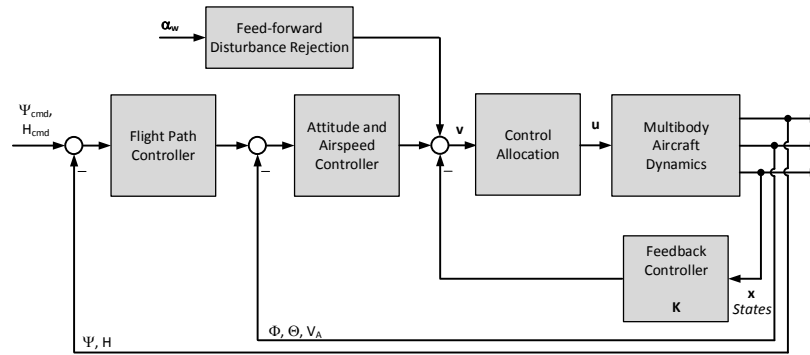


Fig. 3: Flight control law structure for the multibody aircraft

### 3.1 Design Requirements

Tab. 3 summarizes the design requirements for the control law design process. Attitude control requirements (for pitch and bank angle) are taken from SAE AS 94900 [11] and modified slightly, because the multibody aircraft is an unmanned vehicle that is not subject to the full scope of SAE AS 94900. Requirements for azimuth and altitude control are directly taken of SAE AS 94900.

### 3.2 Control Allocation

In Sec. 2.1 it was explained that a formation of ten aircraft with joints that do not transmit rolling and pitching moments has 24 degrees of freedom (3 translational degrees of freedom and 21 rotational degrees of freedom). Every translational degree of freedom is affected by a force while a rotational movement is caused by a moment. Thrust as well as aerodynamic surfaces lead to forces and moments. In total, the multibody aircraft has 50 inputs (cf. Sec. 2.2). That means that there are more inputs available than actually required to influence all degrees of freedom. Such so-called over-actuated systems are handled using control allocation. The main idea of aircraft control allocation is as follows. The control design is not carried out by directly using the aerodynamic surfaces or thrust. Rather, inputs of the aircraft are expressed (indirectly) by moments and forces or their equivalent accelerations and rotational accelerations acting on the aircraft. Those inputs are referred to as *virtual* inputs  $\mathbf{v} \in \mathbb{R}^n$ . The inputs of the aerodynamic surfaces or thrust are denoted as  $\mathbf{u} \in \mathbb{R}^m$  with  $m$  as number of *real* inputs. To establish a relation between the two input types, a mapping is applied:  $\mathbf{B}_a$  transfers the real inputs to the virtual ones by

Table 3: Requirements for the control law design process

No. Requirement	Detailed description	Evidence
1 Nominal stability of all - modes		Eigenvalues of closed-loop system
2 M	The frequency of the formation modes shall be much higher than the rigid-body modes	Eigenvalues of closed-loop system
3 Prevention of stall	The design lift coefficient corresponds to 90 % of the maximum lift coefficient. This means that the maximum drop in airspeed has to be less than $1.7 \frac{m}{s}$ along the complete wing in any maneuver or gust.	Non-linear simulations
4 Pitch angle control performance	90 % of the demanded pitch angle shall be established within 5 s	Non-linear simulations
5 Bank angle control performance	80 % of the demanded bank angle shall be established within 5 s	Non-linear simulations
6 Azimuth control performance	Maximum overshoot of selected azimuth less than $1.5^\circ$ and maximum deviation of $\pm 0.5^\circ$ for azimuth hold	Non-linear simulations
7 Altitude control performance	Selected altitude shall not overshoot by more than 9.14 m	Non-linear simulations
8 Control input limitation	Aerodynamic surfaces (elevator, ailerons and rudder) shall not deflect more than $\pm 30^\circ$ and thrust shall be greater than 0 kW and less than 11.51 kW (cf. Tab 1) for all maneuver and gust	Non-linear simulations

[2]

$$\mathbf{v} = \mathbf{B}_a \mathbf{u} \quad \text{with} \quad \mathbf{B}_a \in \mathbb{R}^{n \times m}. \quad (2)$$

In case of the multibody aircraft, the following 24 virtual inputs are used:

- **3** derivatives of the generalized speeds for the translational motion of the reference aircraft  $u_{kf,AC5}$ ,  $v_{kf,AC5}$ ,  $w_{kf,AC5}$ ,
- **1** derivative of the generalized speed for the yaw motion of the reference aircraft  $r_{kf,AC5}$ ,
- **10** derivatives of the generalized speeds for the roll motion of every aircraft  $p_{kf,AC1-10}$ , and
- **10** derivatives of the generalized speeds for the pitch motion of every aircraft  $q_{kf,AC1-10}$ .

With this, an input for every degree of freedom is available. The mapping matrix  $\mathbf{B}_a$  is determined by the non-linear simulation model. The control law design is now carried out with the state-space system

$$\begin{aligned}\mathbf{x} &= \mathbf{A} \mathbf{x} + \tilde{\mathbf{B}} \mathbf{v} + \mathbf{E} \mathbf{z} \\ \mathbf{y} &= \mathbf{C} \mathbf{x} + \tilde{\mathbf{D}} \mathbf{v} + \mathbf{F} \mathbf{z}\end{aligned}\quad (3)$$

that results from replacing the input vector of Eq. 1 by the transformation of Eq. 2.

Control allocation is thus solving Eq. 2 for  $\mathbf{u}$  [2]. Considering the fact that  $m > n$ , the inverse of  $\mathbf{B}_a$  does not exist. In Sec. 3.6, a method is described to determine the control allocation matrix  $\mathbf{P}$  for

$$\mathbf{u} = \mathbf{P} \mathbf{v} . \quad (4)$$

### 3.3 Inner-Loop Design

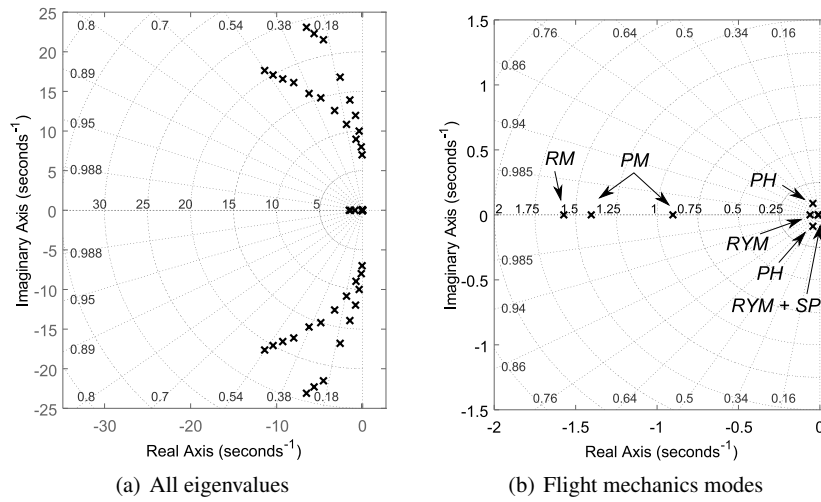


Fig. 4: Eigenvalues of the multibody aircraft's flight dynamics after applying eigenstructure assignment (Kind of rigid-body motion: RM - roll mode, PM - pitch motion(two aperiodic short period modes), RYM - roll-yaw motion, SP - spiral mode, PH - phugoid)

The design of the inner-loop flight control law is carried out by using eigenstructure assignment. Details are provided in Ref. [8]. The designed inner loop separates the formation modes from the rigid-body modes and transforms the highly flexible aircraft formation into a rather rigid-body aircraft. Fig. 4 shows the closed-loop eigenvalues of the multibody aircraft's flight dynamics and inner loop. With this, the first and second design requirement are achieved.

### 3.4 Gust Rejection

In case of a vertical gust, a wind angle of attack

$$\alpha_w = -\arcsin\left(\frac{w_{wg}}{V_A}\right) \quad (5)$$

with  $w_{wg}$  as vertical gust speed occurs. This wind angle of attack increases the angle of attack and may lead to stall. A feed-forward gust rejection element is used to decrease the influence of gust. For the design, the closed-loop system of flight dynamics and inner loop is investigated by step inputs of the wind angle of attack. Those inputs lead to steady pitch angle deviations. To counteract those deviations, an additional pitch rate derivate as virtual input is required. With the step input in the pitch rate derivate, the resulting pitch angle is determined for every aircraft. With this, a relation between wind angle of attack and pitch rate derivate exists to counteract a pitch angle error caused by a vertical gust. The relations for every aircraft are used within the feed-forward gust rejection element. It is assumed that the wind angle of attack is measurable.

### 3.5 Attitude and Airspeed Control Law Design

As the loop for formation control, the attitude and airspeed controller use the virtual inputs. For the first outer loop, those virtual inputs have to be allocated accordingly. A change in pitch angle is connected to a change in the pitch rate. Since formation and rigid-body modes are separated from each other, the change in the pitch rate shall be the same for all aircraft within the formation. This can be established by using a generalized pitch rate derivative  $\dot{q}_{gen, input}$  for all pitch rate derivatives in the virtual control input  $\mathbf{v}$ . This is expressed by

$$\dot{q}_{kf, ACi, input} = \dot{q}_{gen, input} - \dot{q}_{kf, ACi, input, FC} \quad \forall i \in [1, 10] . \quad (6)$$

with  $\dot{q}_{kf, ACi, input}$  as virtual pitch rate derivative input in the control allocation matrix and  $\dot{q}_{kf, ACi, input, FC}$  as pitch rate derivative of the formation control (inner loop). The same approach is used for the bank angle control law. Now, a generalized roll rate derivative  $\dot{p}_{gen, input}$  is used as a common input for all virtual inputs of the roll rate derivatives with

$$\dot{p}_{kf, ACi, input} = \dot{p}_{gen, input} - \dot{p}_{kf, ACi, input, FC} \quad \forall i \in [1, 10] . \quad (7)$$

For airspeed control, the generalized speed derivative  $\dot{u}_{kf, AC5, input}$  is used. The allocation follows from

$$\dot{u}_{kf, AC5, input} = \dot{u}_{kf, AC5, gen} - \dot{u}_{kf, AC5, input, FC} \quad (8)$$

with  $\dot{u}_{kf, AC5, gen}$  as output of the airspeed controller and  $\dot{u}_{kf, AC5, input, IL}$  as output of the inner loop.

The design of the control laws is conducted in the frequency domain. By applying the Laplace transformation, the state-space model of Eq. 3 without disturbances and considering of the inner-loop control law  $\mathbf{K}$  with

$$\tilde{\mathbf{A}} = \mathbf{A} - \mathbf{B} \mathbf{K} \quad (9)$$

yields the system

$$\begin{aligned} s \hat{\mathbf{x}}(s) &= \tilde{\mathbf{A}} \hat{\mathbf{x}}(s) + \mathbf{B} \hat{\mathbf{v}}(s) \\ \hat{\mathbf{y}}(s) &= \mathbf{C} \hat{\mathbf{x}}(s) + \mathbf{D} \hat{\mathbf{v}}(s) \end{aligned} \quad (10)$$

Hence, the transfer function of the plant for control design is determined by

$$\mathbf{G}(s) = \hat{\mathbf{y}}(s) \hat{\mathbf{v}}^{-1}(s) = \mathbf{C} [s \mathbf{I} - \tilde{\mathbf{A}}]^{-1} \mathbf{B} + \mathbf{D}. \quad (11)$$

### 3.5.1 Bank Angle Control Law

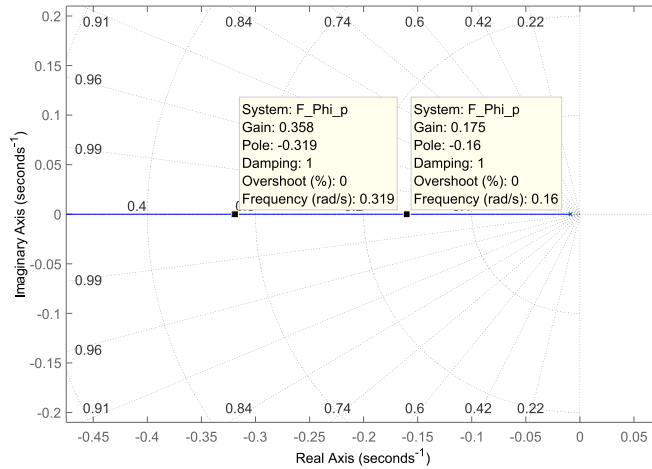


Fig. 5: Root locus  $\dot{p}_{gen, input} \rightarrow \Phi_{ref}$

The bank angle control law is designed as a Single Input Single Output system using the root locus method. At first, the transfer function from the generalized roll rate derivative  $\dot{p}_{gen, input}$  to the bank angle of the reference aircraft  $\Phi_{ref}$  is determined by Eq. 11. Then, the transfer function order is reduced by applying the balanced truncation [3]. The system can be reduced to first order. Considering the fifth requirement of Tab. 3, a time constant for this eigenvalue of  $T = 3.1$  s is re-

quired to reach 80 % of the steady value after 5 s. The transfer function of the reduced system is calculated. The root locus plot is shown in Fig 5. To meet the design criterion, a gain of  $k_{p,\phi} = 0.358$  is required. After a set of linear simulation studies and optimized control allocation (cf. Sec. 3.6), it turned out that the limits of the aerodynamic control surfaces are exceeded by a factor of 1.9. Hence, this pole placement is not possible. The lowest selectable value is a pole with a time constant of  $T = 6.25$  s and a corresponding gain of  $k_{p,\phi} = 0.175$ .

### 3.5.2 Pitch and Airspeed Control Law

Because airspeed control is very important, a Multiple Input Multiple Output control law design for the airspeed and pitch control law is conducted in the frequency domain by using  $\mathcal{H}_\infty$ -loop shaping. The designed bank angle control law is included in the system of Eq. 11 and a new plant model

$$\begin{bmatrix} V_A \\ \Theta \end{bmatrix} = \mathbf{G}_2 \begin{bmatrix} \dot{u}_{\text{kf, AC5, gen}} \\ \dot{q}_{\text{gen, input}} \\ \Phi_{\text{cmd}} \end{bmatrix} \quad (12)$$

is built that is used for the design of the airspeed and pitch control law. In Eq. 12, the demanded bank angle  $\Phi_{\text{cmd}}$  is considered as disturbance. The  $\mathcal{H}_\infty$ -loop shaping is well described in the literature [14, 12, 6]. Consequently, only the central parts of the design method are described in the present paper. At first, the input and output of Eq. 12 are normalized to the maximum accepted values. The maximum accepted inputs are

$$\dot{u}_{\text{kf, AC5, gen, max}} = 0.25 \text{ m s}^{-2} \quad \text{and} \quad \dot{q}_{\text{gen, input, max}} = 0.25^\circ \text{ s}^{-2}.$$

The maximum velocity error is defined as  $0.1 \frac{\text{m}}{\text{s}}$  and pitch angle error as  $1^\circ$ . Considering the maximum yaw rate and the airspeed, a maximum bank angle of  $2.98^\circ$  is used to avoid stall of the aircraft that flies turn-inwards. The normalized system is used to shape the sensitivity function

$$\mathbf{S} = (\mathbf{I} + \mathbf{G} \mathbf{K})^{-1} \quad (13)$$

with  $\mathbf{G}$  as plant and  $\mathbf{K}$  as controller. The sensitivity function describes with

$$\mathbf{e} = \mathbf{S}(\mathbf{r} - \mathbf{d}) \quad (14)$$

how a reference signal  $\mathbf{r}$  and a disturbance signal  $\mathbf{d}$  influence the control error  $\mathbf{e}$  in the frequency domain. If the magnitude of the sensitivity function is greater than one, the closed-loop system performance is worse than without a controller. For the loop shaping, a design weight  $w_S$  is used

$$w_S = \frac{\frac{s}{M} + \omega_{BW}}{s + \omega_{BW} A}, \quad (15)$$

where  $\omega_{BW}$  is the bandwidth,  $A$  is the lower bound and  $M$  is the upper bound for the sensitivity function [12]. The inverse of the design weight in Eq. 15 represents the desired sensitivity function. The parameters for the weight  $w_S$  are listed in Tab. 4 for the airspeed and pitch angle. The desired bandwidth corresponds to the design requirements of Tab. 3. In addition, the inputs are shaped with an identity matrix. The  $\mathcal{H}_\infty$ -loop shaping is applied and a maximum norm of 1.645 is computed. The order of the resulting control law is ten. The inverse normalization is computed for the control law and the system is integrated in the attitude and airspeed controller of Fig. 3.

Table 4: Parameters of the sensitivity weights

Output	Bandwidth $\omega_{BW} \left[ \frac{\text{rad}}{\text{s}} \right]$	Lower bound $A \text{ [dB]}$	Upper bound $M [-]$
Airspeed	0.458	-80	1.75
Pitch angle	0.458	-80	1.75

### 3.6 Solving the Control Allocation Problem

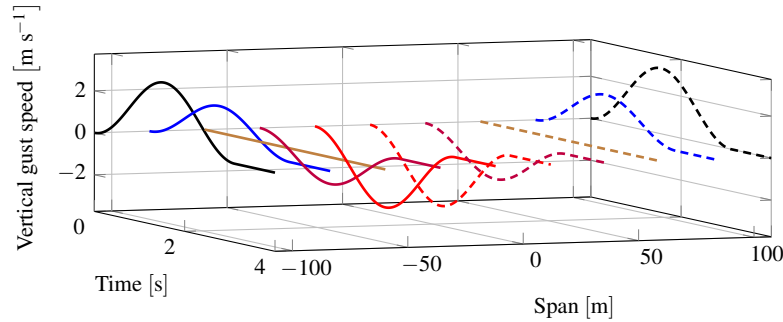


Fig. 6: Vertical wind speed profile for all aircraft's center of gravity using a DARPA gust

The designed control laws directly command the virtual inputs in the flight dynamic, while the outer loop for altitude and heading control commands desired pitch and bank angle to the attitude control law. Therefore, the control allocation problem

of Eq. 4 is now solved. The solution of the control allocation problem shall comply with the maximum allowable real inputs for the reference test cases. Those test cases are

1. Step input in the pitch angle command of  $1^\circ$ ,
2. Step input in the bank angle command of  $2.9^\circ$ , and
3. DARPA gust acting [1] on the multibody aircraft.

Fig. 6 shows the used DARPA gust. Details of the calculation are provided in [1].

A frequently used solution for the control allocation is the Moore-Pensorse pseudo-inverse. This pseudo-inverse reduces the 2-norm of the control vector  $\|\mathbf{u}\|_2$ . It arises from

$$\mathbf{u} = \underbrace{\mathbf{B}_a^T [\mathbf{B}_a \mathbf{B}_a^T]^{-1}}_{\mathbf{P}} \mathbf{v} \quad (16)$$

as a solution of the control allocation with  $\mathbf{P}$  as pseudo-inverse [2]. Instead of minimizing  $\mathbf{u}^T \mathbf{u}$ , a weighting matrix  $\mathbf{W}$  can be used to take different control efforts and the maximum and minimum boundaries of the real inputs into account. This method was successfully used for the inner loop [8]. For the reference test case, the boundaries of the real inputs are violated with this method. Therefore another approach is used.

To select a suitable weighting matrix  $\mathbf{W}$ , a numerical optimization of the weighting matrix is carried out. The procedure is shown in Fig. 7. A weighting matrix is determined, the control allocation problem is solved and linear simulation studies are carried out for all test cases. For every control input, the maximum and minimum values are calculated and normalized using the previously introduced maximum and minimum values for all three simulation runs. Those values are used as design criteria that have to be smaller than one. The optimization is carried out with the toolbox MOPS (*Multi-Objective Parameter Synthesis*) of the German Aerospace Center (DLR) [4] and stops if all criteria are smaller or equal to one. With this method, a suitable solution for the control allocation problem is found.

### 3.7 Flight Path Control Law Design

The flight path is controlled by an altitude  $H$  and azimuth  $\Psi$  controller. The transfer functions  $G_{H \Theta_{\text{cmd}}}$  and  $G_{\Psi \Phi_{\text{cmd}}}$  obtained from the closed-loop system of multibody aircraft flight dynamics, inner-loop, attitude and airspeed control are used for the control law design. Altitude control is established with the proportional control law

$$\Theta_{\text{cmd}} = k_{\Theta_{\text{cmd}} H} (H_{\text{cmd}} - H) . \quad (17)$$

For gain determination, the open-loop transfer function  $G_{H \Theta_{\text{cmd}}}$  is shown in the Bode diagram and the gain factor is changed to meet a phase margin of minimum

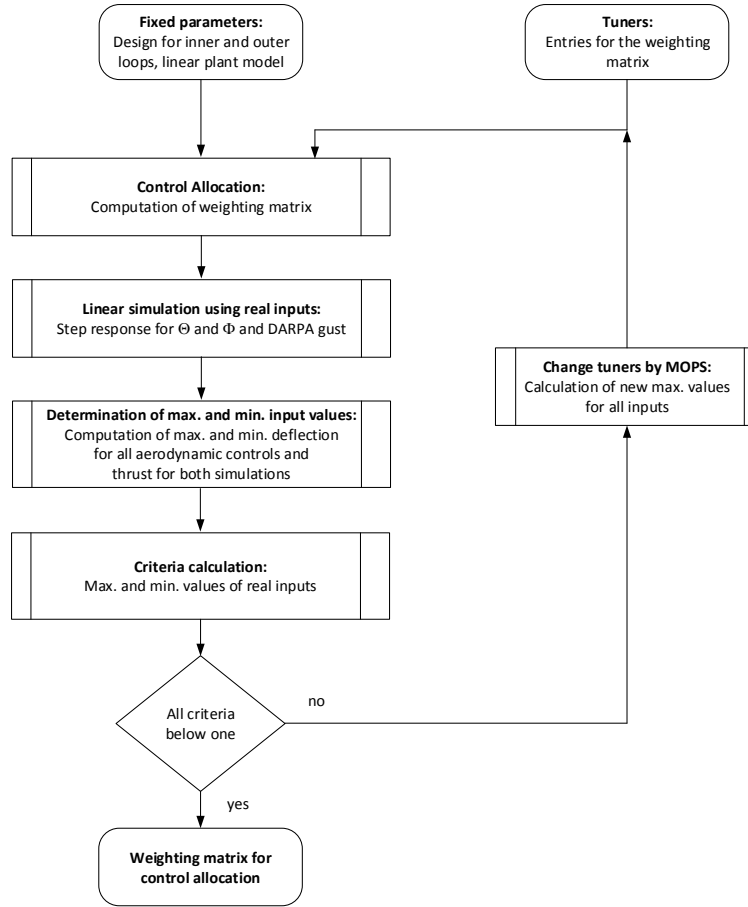


Fig. 7: Flow chart to optimize the weighting matrix  $\mathbf{W}$  of the control allocation problem to achieve suitable aerodynamic surface deflection and thrust

$45^\circ$  and a gain margin of minimum 3 dB according to SAE AS 94900. The same design procedure is applied to the azimuth control law. The control law

$$\Phi_{\text{cmd}} = k_{\Phi_{\text{cmd}}} \psi (\Psi_{\text{cmd}} - \Psi), \quad (18)$$

is used and the gain  $k_{\Phi_{\text{cmd}}} \psi$  is set to meet the design goals of phase and gain margin with minimum  $45^\circ$  and 3 dB.

The commanded pitch angle  $\Theta_{\text{cmd}}$  is bounded between  $-1^\circ$  and  $1^\circ$ . The maximum commanded bank angle interval is between  $-2.9^\circ$  and  $2.9^\circ$ . With those limitations, the minimum and maximum real control inputs are not violated.

## 4 Non-linear Simulation Results

The designed control laws are now tested within the non-linear simulation environment. In the first test case, a DARPA gust acts on the aircraft. For this test case, only the attitude and airspeed controller, the inner-loop and feed-forward gust rejection element are used. The second test case is an azimuth step input and in the third test case a step input in the demanded altitude is tested.

### 4.1 DARPA Gust

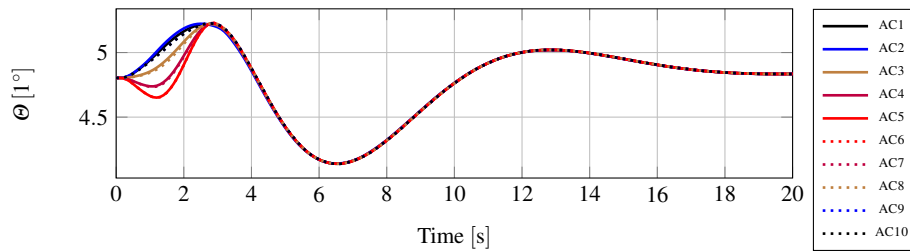


Fig. 8: Non-linear response of all pitch angles in case of DARPA gust

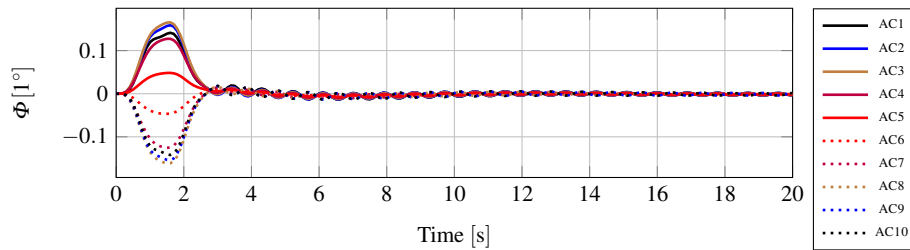


Fig. 9: Non-linear response of all bank angles in case of DARPA gust

Selected non-linear results for the DARPA gust are shown in Fig. 8 to Fig. 15. The pitch angle response in Fig. 8 shows that the inner aircraft (AC4 to AC7) performs a pitch down motion, while the outer aircraft pitches the nose up during the gust. This is the desired behavior established by the feed-forward gust rejection element. After the gust, all pitch angles are in phase and have the same magnitude. Changes in the bank angle are very small as shown in Fig. 9. The airspeed control law also works very well. Figure 10 shows deviations of maximum  $0.2 \text{ m s}^{-1}$  full-

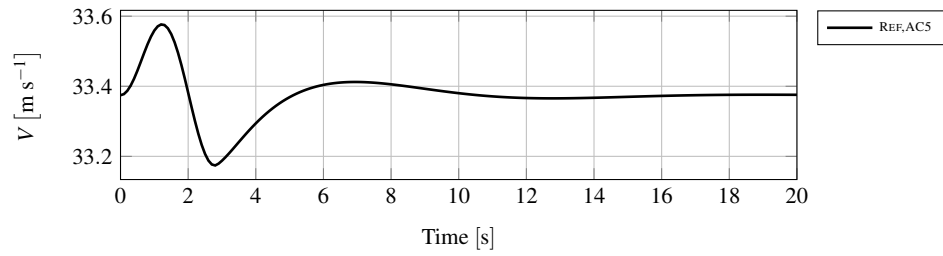


Fig. 10: Non-linear response of airspeed in case of DARPA gust

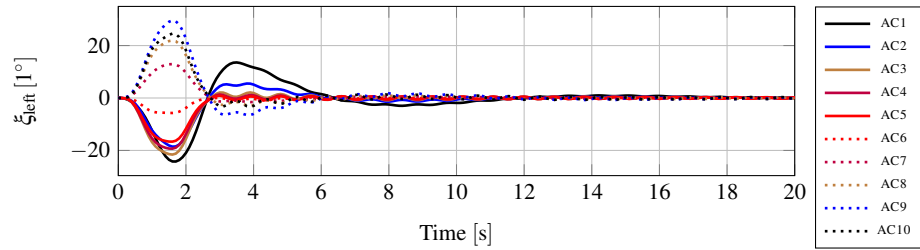


Fig. 11: Non-linear response of all left ailerons in case of DARPA gust

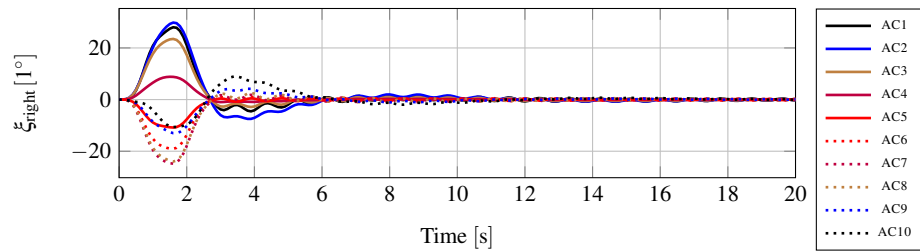


Fig. 12: Non-linear response of all right ailerons in case of DARPA gust

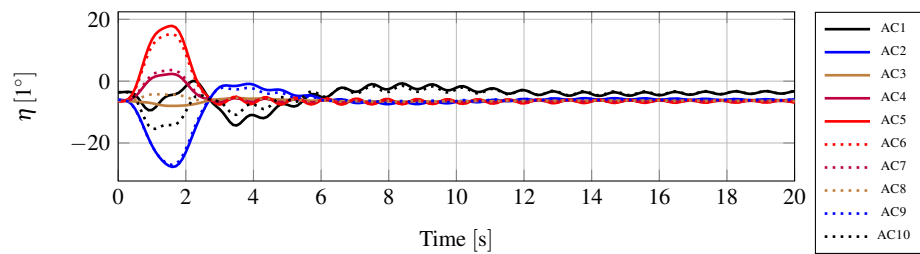


Fig. 13: Non-linear response of all elevators in case of DARPA gust

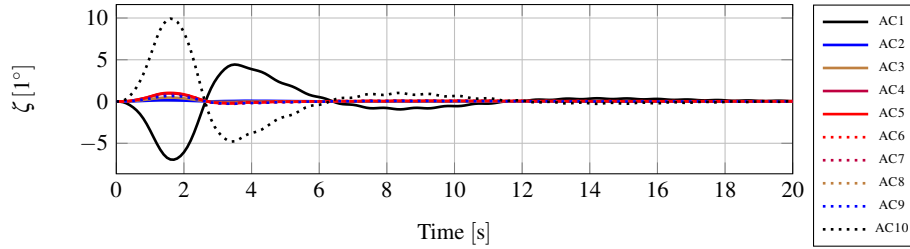


Fig. 14: Non-linear response of all rudders in case of DARPA gust

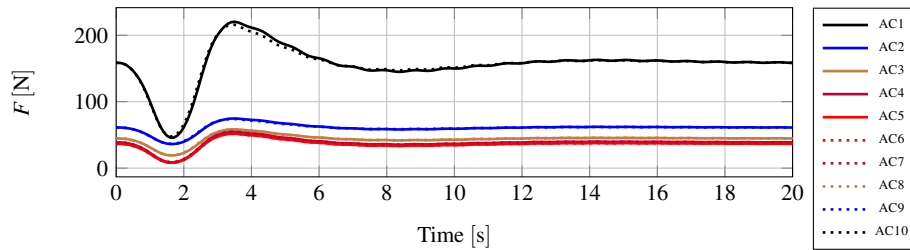


Fig. 15: Non-linear response of all engines in case of DARPA gust

filling the third requirement of Tab. 3. The aerodynamic control surfaces (cf. Fig. 11 to Fig. 14) as well as the thrust (cf. Fig. 15) are within the limits. This shows the successful solution of the control allocation problem and, confirms achievement of the eighth design criterion of Tab. 3.

## 4.2 Azimuth Change

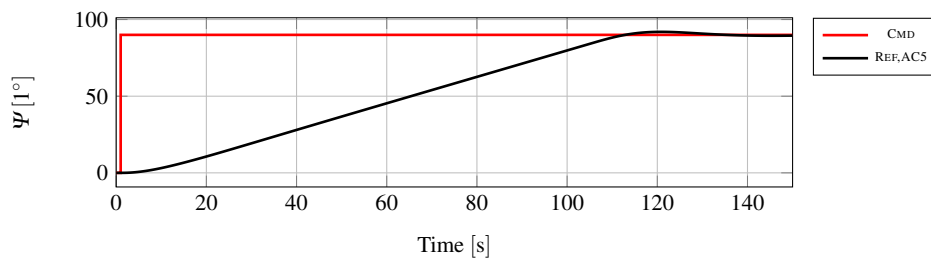


Fig. 16: Non-linear response of the azimuth in case of an azimuth step input

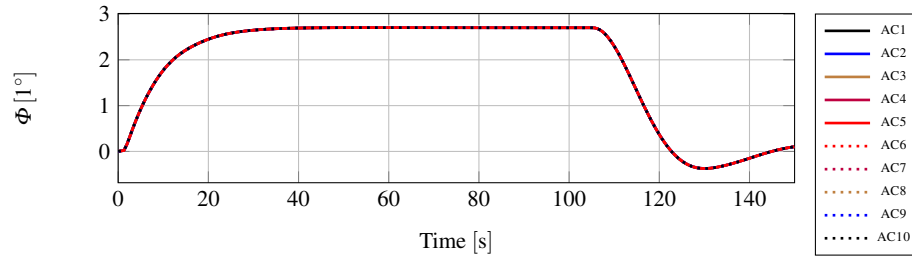


Fig. 17: Non-linear response of all bank angles in case of an azimuth step input

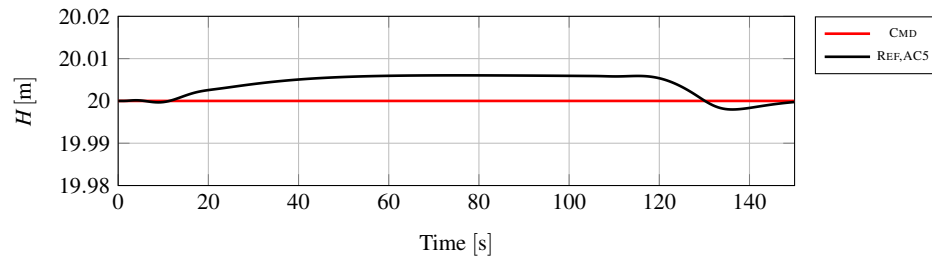


Fig. 18: Non-linear response of the altitude in case of an azimuth step input

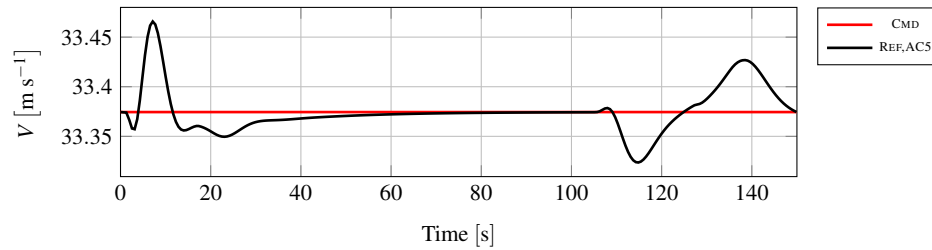


Fig. 19: Non-linear response of airspeed in case of an azimuth step input

The non-linear response of selected parameters for a step input azimuth command of  $90^\circ$  is shown in Fig. 16 to 19. A maximum overshoot of  $1.97^\circ$  occurs in the azimuth, see Fig. 16. This fulfills the sixth requirement of Tab. 3. Figure 17 shows the bank angles that are all in phase and have the same magnitude because of the inner loop. The maximum overshoot in the altitude is 6.05 m (cf. Fig. 18). With this, the seventh requirement of Tab. 3 is also fulfilled. The airspeed that is shown in Fig. 19 is held with high accuracy and, hence, there will be no stall in turned flight condition.

### 4.3 Altitude Change

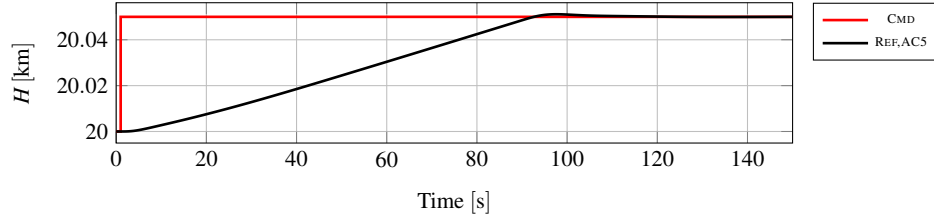


Fig. 20: Non-linear response of the altitude in case of an altitude step input

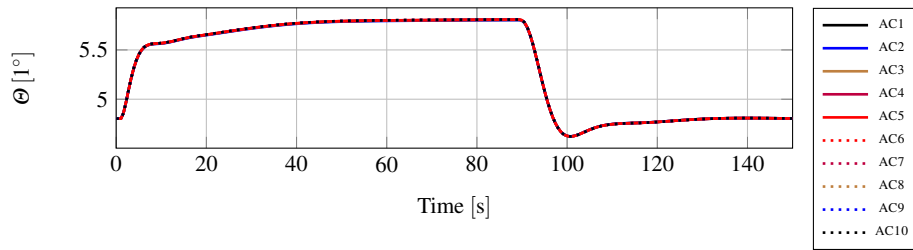


Fig. 21: Non-linear response of all pitch angles in case of an altitude step input

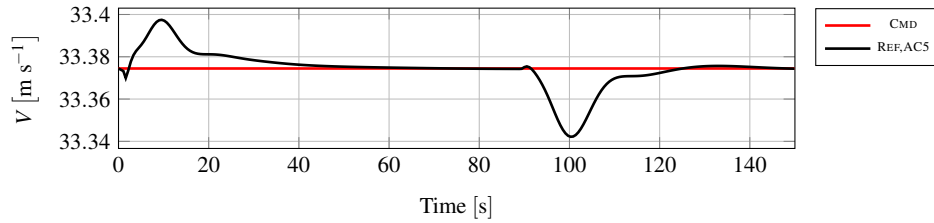


Fig. 22: Non-linear response of the airspeed in case of an altitude step input

In this test case, an altitude step of 50 m is commanded. Selected parameters of the non-linear simulation are shown in Fig. 20 to Fig. 22. Figure 20 shows the altitude response. An overshoot of 1.13 m occurs that fulfills the seventh requirement of Tab. 3. The pitch angle response is shown in Fig. 21. All pitch angles have the same phase and magnitude. This emphasizes the very good performance of the inner loop with respect to the separation of rigid-body modes and formation modes. Changes in the airspeed (cf. Fig. 22) are very low and there is no risk of stall.

## 5 Conclusion

This paper provides a sequential design method of the outer loops for aircraft with a very high wing span using the multibody aircraft as example. With well-designed inner loop, the formation of multiple linked single aircraft can be transformed to a nearly rigid-body aircraft with a clear separation between rigid-body modes and formation modes. With this, the classical cascade flight control law structure can be applied to multibody aircraft as well. Considering the bank angle control law in the design of the airspeed control law, airspeed can be held with high accuracy even in turns. This prevents stall and ensures a safe operation. The method was applied for a multibody aircraft. In general, the design procedure can be also applied for highly flexible aircraft with a single wing with high aspect ratio.

## References

1. Dillsaver, Matthew and Cesnik, Carlos and Kolmanovsky, Ilya, *Gust response sensitivity characteristics of very flexible aircraft*, AIAA Atmospheric Flight Mechanics Conference, 2012
2. Durham, Wayne and Bordignon, Kenneth A and Beck, Roger, *Aircraft control allocation*, John Wiley & Sons, 2017.
3. Gu, Da-Wei and Petkov, Petko and Konstantinov, Mihail M., *Robust control design with MATLAB®*, Springer, 2015
4. Joos, Hans-Dieter, *Multi-objective parameter synthesis (MOPS)*, in: *Robust Flight Control*, Springer, 1997
5. Kane, Thomas R., Levinson, David A., *Dynamics, theory and applications*, McGraw Hill, 1985.
6. Köthe, Alexander, and Luckner, Robert, and Ramirez, Pedro J.G., and Silvestre, Flavio, and Pang, Zi Y., and Cesnik, Carlos, *Development of Robust Flight Control Laws for a Highly Flexible Aircraft in the Frequency Domain*, AIAA Atmospheric Flight Mechanics Conference, 2016
7. Köthe, Alexander, and Luckner, Robert, *Flight Path Control for a Multi-body HALE Aircraft*, in: *Aerospace Guidance, Navigation and Control*, Springer, 2018
8. Köthe, Alexander, and Luckner, Robert, *Applying Eigenstructure Assignment to Inner-Loop Flight Control Laws for a Multibody Aircraft*, submit as contribution to the EuroGNC 2019
9. Levine, William S, *The Control Systems Handbook: Control System Advanced Methods*, CRC press, 2010.
10. Lockett, B., *Flying Aircraft Carriers of the USAF: Wing Tip Coupling*, LockettBooks, 2013.
11. Society of Automotive Engineers, *Aerospace Standard AS94900, Flight Control Systems*, SAE International, 2007
12. Skogestad, Sigurd and Postlethwaite, Ian, *Multivariable feedback control: analysis and design*, Vol. 2, John Wiley & Sons, 2007.
13. Sommer, Geoffrey S, *Modular articulated-wing aircraft*, US Patent 9,387,926, 2016.
14. Zames, George, *Feedback and optimal sensitivity: Model reference transformations, multiplicative seminorms, and approximate inverses*, IEEE Transactions on Automatic Control, Vol. 26, 1981